

# HIGGS-RADION INTERPRETATION OF 750 GeV DI-PHOTON EXCESS AT THE LHC

Aqeel Ahmed,<sup>a,b</sup> Barry M. Dillon,<sup>c</sup> Bohdan Grzadkowski,<sup>a</sup>  
John F. Gunion,<sup>d</sup> and Yun Jiang<sup>e</sup>

<sup>a</sup>*Faculty of Physics, University of Warsaw, Pasteura 5, 02-093 Warsaw, Poland*

<sup>b</sup>*National Centre for Physics, Quaid-i-Azam University Campus, Islamabad, Pakistan*

<sup>c</sup>*Department of Physics and Astronomy, University of Sussex, BN1 9QH Brighton, U.K.*

<sup>d</sup>*Department of Physics, University of California, Davis, CA 95616, U.S.A.*

<sup>e</sup>*NBIA and Discovery Center, Niels Bohr Institute, University of Copenhagen, Blegdamsvej 17,  
DK-2100, Copenhagen, Denmark*

aqeel.ahmed@fuw.edu.pl, b.dillon@sussex.ac.uk, bohdan.grzadkowski@fuw.edu.pl,  
gunion@physics.ucdavis.edu, yunjiang@nbi.ku.dk

---

**ABSTRACT:** We present a possible interpretation of the excess in the di-photon channel at 750 GeV recently observed by ATLAS and CMS as the radion of the five-dimensional Randall-Sundrum model. We show that the Higgs-radion scenario can give a cross section of  $(5 - 15)$  fb in the di-photon final state at 750 GeV while at the same time giving a very SM-like state at 125 GeV.

---

**KEYWORDS:** Beyond Standard Model, Warped Extra Dimensions, Higgs-Radion

---

## Contents

<b>1</b>	<b>Introduction</b>	<b>1</b>
<b>2</b>	<b>Phenomenology of the 750 GeV Higgs-radion</b>	<b>3</b>
<b>3</b>	<b>Conclusions</b>	<b>8</b>
<b>A</b>	<b>Holographic interpretation: a 750 GeV dilaton</b>	<b>9</b>
<b>B</b>	<b>Electroweak precision constraints on <math>m_1^g</math></b>	<b>10</b>

---

## 1 Introduction

At the LHC, recently the ATLAS [1] and CMS [2] collaborations have presented their first results on the di-photon final state at energy  $\sqrt{s} = 13$  TeV. Both collaborations have found a narrow excess over the background in the di-photon ( $\gamma\gamma$ ) final state at  $\sim 750$  GeV. The local significances of this signal at the di-photon invariant mass  $m_{\gamma\gamma} \approx 750$  GeV are  $3.9\sigma$  and  $2.6\sigma$  for the ATLAS and CMS collaborations, respectively. We summarize the LHC data in Table 1 for the excess observed above expected background over an interval centered on  $m_{\gamma\gamma} \approx 750$  GeV. Meanwhile, it is important to note that no excess is observed in any other channels, including the  $t\bar{t}$ ,  $hh$ ,  $WW$ ,  $ZZ$  and di-jet final states. In this report, we present a possible interpretation of this signal using the mixed *Higgs-radion* sector of the Randall-Sundrum (RS) model.

**Table 1:** Summary of the LHC di-photon excess at the invariant mass of  $\sim 750$  GeV from the ATLAS [1] and CMS [2] collaborations at energy  $\sqrt{s} = 13$  TeV ( $\sigma$  is the local statistical significance).

	ATLAS @ $\sqrt{s} = 13$ TeV [1]	CMS @ $\sqrt{s} = 13$ TeV [2]
Excess Events	14 with $3.9\sigma$	10 with $2.6\sigma$
$\sigma(pp \rightarrow \gamma\gamma)$	$(10 \pm 3)$ fb	$(6 \pm 3)$ fb

The Randall-Sundrum (RS) model [3] consists of one extra spatial dimension bounded by two 3-branes; this can be viewed either as a finite interval or as an  $S_1/Z_2$  orbifold. In the limit of no back-reaction, the bulk background geometry is anti-de Sitter (AdS) space and the spectrum contains a massless radion. It has been shown that the Goldberger-Wise mechanism is successful in both stabilising the size of the inter-brane distance in this model and in giving the radion a mass [4, 5]. In this work we will consider an effective theory where the radion is massive. Moreover, we will neglect the effects of the back-reaction upon the metric. In the notation of Refs. [6–8] the 5D metric has the following form,

$$ds^2 = e^{-2kb_0|y|} \eta_{\mu\nu} dx^\mu dx^\nu - b_0^2 dy^2, \quad (1.1)$$

where  $k$  is the curvature of the 5D geometry,  $b_0$  is the length along the extra-dimension, and  $-1/2 \leq y \leq 1/2$ . The fluctuation of the 55-component associated with  $b_0$  is referred as the radion,  $\phi_0(x)$ . The literature on radion models is extensive, but can be conveniently separated into three model categories – namely those with: the SM on the IR brane [9]; the SM in the bulk but the Higgs on the IR brane [8–10]; the full SM (including the Higgs) in the bulk [11]. In this study we consider the SM in the bulk, plus a custodial symmetry [12], with the Higgs localised on the IR brane. Thus the local symmetry in the bulk will be  $SU(2)_L \times SU(2)_R \times U(1)_X$ , where the  $SU(2)_R \times U(1)_X$  fields are broken to  $U(1)_Y$  on the UV brane, such that  $Y = T_R^3 + X$ . This custodial symmetry allows us to obtain a lower scale for the new physics resonances (KK-modes) without violating bounds coming from the electroweak precision observables (EWPO).

Since we have a brane Higgs, the Higgs-gravity coupling ( $\xi \mathcal{R}_4 H^\dagger H$ ) can only be induced on the IR brane. This results in the following four-dimensional (4D) effective Lagrangian for the scalar sector,

$$\mathcal{L}_{\text{eff}} = \frac{1}{2}(\partial_\mu \phi_0)^2 - \frac{1}{2}m_{\phi_0}^2 \phi_0^2 - 6\xi \Omega \square \Omega H^\dagger H + |D_\mu H|^2 - \Omega^4 V(H), \quad (1.2)$$

where  $\xi$  is a dimensionless parameter that defines the non-trivial Higgs-gravity coupling [13]. Above we have defined  $\Omega(\phi_0) \equiv 1 - \ell \phi_0/v_0 + \mathcal{O}(\ell^2)$ , where  $\ell \equiv v_0/\Lambda_\phi$  with  $v_0 = 246$  GeV and  $\Lambda_\phi \equiv \sqrt{6}M_{\text{Pl}}e^{-kb_0/2}$ .

We can rewrite the above Higgs-radion Lagrangian at the quadratic level as,

$$\mathcal{L}_{\text{eff}}^{(2)} = -\frac{1}{2}(1 + 6\xi\ell^2)\phi_0\square\phi_0 - \frac{1}{2}m_{\phi_0}^2\phi_0^2 + 6\xi\ell h_0\square\phi_0 - \frac{1}{2}h_0\square h_0 - \frac{1}{2}m_{h_0}^2 h_0^2, \quad (1.3)$$

where  $h_0$  is the neutral scalar of the Higgs doublet  $H$ , and  $m_{h_0}$  is the bare Higgs mass. In the above Lagrangian the  $\xi$  term that mixes the Higgs and the radion can be removed by rotating the scalar fields into the mass eigenstate basis as,

$$\begin{pmatrix} \phi_0 \\ h_0 \end{pmatrix} = \begin{pmatrix} -a & -b \\ c & d \end{pmatrix} \begin{pmatrix} \phi \\ h \end{pmatrix}, \quad (1.4)$$

where  $a = -\cos\theta/Z$ ,  $b = \sin\theta/Z$ ,  $c = \sin\theta + t\cos\theta$  and  $d = \cos\theta - t\sin\theta$ , with  $t \equiv 6\xi\ell/Z$ ,  $Z \equiv 1 + 6\xi\ell^2(1 - 6\xi)$  and

$$\tan 2\theta = \frac{12\xi\ell Z m_{h_0}^2}{m_{\phi_0}^2 - m_{h_0}^2(Z^2 - 36\xi^2\ell^2)}. \quad (1.5)$$

To maintain a positive definite kinetic energy for the radion we require that,

$$\frac{1}{12} \left( 1 - \sqrt{1 + \frac{4}{\ell^2}} \right) \leq \xi \leq \frac{1}{12} \left( 1 + \sqrt{1 + \frac{4}{\ell^2}} \right). \quad (1.6)$$

As long as  $\ell$  is small the physical masses are only corrected up to  $\mathcal{O}(\ell^2)$  from their bare values before mixing, which is indeed the case for  $\ell \leq 1/(6\sqrt{6})$  when  $\Lambda_\phi \geq 1.5$  TeV, which

**Table 2:** Couplings of the SM particles with the Higgs  $h(x)$  and the radion  $\phi(x)$  (complete list can be found in [6]). Above we defined  $g_h \equiv (d + \ell b)$ ,  $g_\phi \equiv (c + \ell a)$ ,  $g_h^r \equiv \ell b$  and  $g_\phi^r \equiv \ell a$ .

	$h(x)$	$\phi(x)$
$WW$	$gm_W g_h$	$gm_W g_\phi$
$ZZ$	$\frac{gm_Z}{c_W} g_h$	$\frac{gm_Z}{c_W} g_\phi$
$\gamma\gamma$	$\frac{\alpha}{2\pi v_0} \left[ g_h^r \left( b_2 + b_Y + \frac{2\pi}{\alpha k b_0/2} \right) - g_h \sum_i e_i^2 N_c^i F_i(\tau_i) \right]$	$\frac{\alpha}{2\pi v_0} \left[ g_\phi^r \left( b_2 + b_Y + \frac{2\pi}{\alpha k b_0/2} \right) - g_\phi \sum_i e_i^2 N_c^i F_i(\tau_i) \right]$
$gg$	$\frac{\alpha_s}{4\pi v_0} \left[ 2g_h^r \left( b_3 + \frac{2\pi}{\alpha_s k b_0/2} \right) - g_h \sum_i F_{1/2}(\tau_i) \right]$	$\frac{\alpha_s}{4\pi v_0} \left[ 2g_\phi^r \left( b_3 + \frac{2\pi}{\alpha_s k b_0/2} \right) - g_\phi \sum_i F_{1/2}(\tau_i) \right]$
$f\bar{f}$	$\frac{g}{2} \frac{m_f}{m_W} g_h$	$\frac{g}{2} \frac{m_f}{m_W} g_\phi$
$Z\gamma$	$(\text{SM-coupling})^* g_h$	$(\text{SM-coupling})^* g_\phi$

is required by the EWPO and  $k/M_{\text{Pl}} \leq 2$ , see Fig. 1. It is instructive to rewrite Eq. (1.5) in terms of the physical mass parameters as

$$\tan 2\theta = \frac{12\xi \ell m_{h_0}^2}{Z(m_\phi^2 + m_h^2 - 2m_{h_0}^2)} \simeq 2\ell \frac{m_h^2}{m_\phi^2} \frac{6\xi}{Z} + \mathcal{O}(\ell^3), \quad (1.7)$$

where  $m_{h_0}^2 = 2\lambda v_0^2$ , with  $\lambda$  being the Higgs quartic coupling.

For the present paper, the most important point to note from the earlier studies, see e.g. [6–8, 10, 13], is that the coupling of the radion to the trace of the energy momentum tensor leads to the existence of a special choice of  $\xi$  where the radion’s couplings to the SM particles other than  $\gamma\gamma$  and  $gg$  are suppressed while the  $\phi\gamma\gamma$  and  $\phi gg$  couplings have extra “anomalous” contributions that are not suppressed. (We summarize the most relevant couplings for our purpose in Table 2 — one can find the complete list of couplings and the definitions of our parameters in Ref. [6].) As a result, for this special choice of  $\xi$  it is possible for the radion to be strongly produced by  $gg$  fusion with primary decay to  $gg$  (a di-jet final state) but also with significant branching ratio for decay to  $\gamma\gamma$ . Amusingly, the special choice of  $\xi$  for which this situation arises when  $m_\phi \gg m_h$  is close to the conformal limit of  $\xi = 1/6$ .

## 2 Phenomenology of the 750 GeV Higgs-radion

Apart from the mixing, the strength of the couplings between the radion and SM fields are controlled by the mass of the lightest KK-gluon ( $m_1^g$ ), and  $k/M_{\text{Pl}}$ . Bounds on  $m_1^g$  are typically  $\sim 3$  TeV [15, 16]; we refer the reader to Appendix B for more details. The ratio  $k/M_{\text{Pl}}$  is typically assumed to be small. However, in Ref. [14] it has been argued that  $k/M_{\text{Pl}} < \sqrt{3\pi^3/5\sqrt{5}} \sim 3$  is acceptable. Note that the first KK-gluon mass  $m_1^g$  is related to  $\Lambda_\phi$  and  $k/M_{\text{Pl}}$  as follows:

$$m_1^g = \frac{x_1^g}{\sqrt{6}} \frac{k}{M_{\text{Pl}}} \Lambda_\phi, \quad \text{with} \quad kb_0 = 2 \ln \left( \frac{\sqrt{6} M_{\text{Pl}}}{\Lambda_\phi} \right), \quad (2.1)$$

where  $x_1^g \simeq 2.45$  is the 1st zero of an appropriate Bessel function [6]. In Fig. 1 we show the contours of  $\Lambda_\phi$  in the  $(m_1^g, k/M_{\text{Pl}})$  plane, where the region below  $m_1^g = 3$  TeV (dashed-red line) is excluded by the Electroweak Precision Observations (EWPO), see Fig. 7. In order



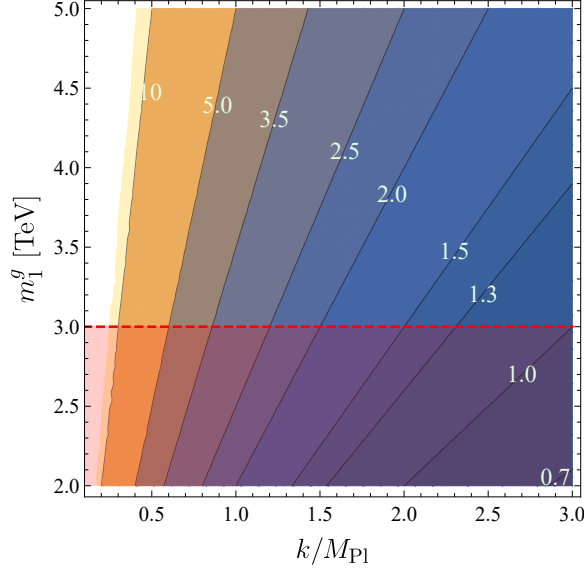


**Figure 1:** Correlation between  $m_1^g$  and  $k/M_{\text{Pl}}$  for different contours of  $\Lambda_\phi$  (in the unit of TeV). The region below  $m_1^g = 3$  TeV (dashed-red line) is excluded by the EWPO.

to satisfy the EWPO constraints we employ a custodial symmetry  $SU(2)_L \times SU(2)_R$  in the bulk which is broken to the SM subgroup on the UV brane. These constraints are obtained by assuming that the contributions from the Higgs-radion sector are small and hence the main contributions come from the effects of the KK top quarks and the bulk  $SU(2)_R$  breaking. The details are supplemented in Appendix B. Note that for a conservative value of  $k/M_{\text{Pl}} \leq 2$ , there is bound on the  $\Lambda_\phi \geq 1.5$  TeV and  $\Lambda_\phi \geq 2.5$  TeV for  $m_1^g = 3$  TeV and  $m_1^g = 5$  TeV, respectively. However, if we take the maximal value  $k/M_{\text{Pl}} \leq 3$ , suggested in Ref. [14], then the bound on  $\Lambda_\phi \geq 1$  TeV and  $\Lambda_\phi \geq 1.7$  TeV for  $m_1^g = 3$  TeV and  $m_1^g = 5$  TeV, respectively.

As stated in the Introduction, we will show that the recent LHC excess at 750 GeV in the di-photon channel can be explained if the radion eigenstate ( $\phi$ ) has this mass. Meanwhile, the primarily  $h_0$  eigenstate state,  $h$ , can be chosen to have  $m_h = 125$  GeV. In addition, we choose  $m_1^g = 2.5, 3, 5$  TeV and require  $\Lambda_\phi \geq 1.5$  TeV, such values being consistent with bounds from the direct searches [15, 16] and allowed by the EWPO, see Fig. 7. We first display in Fig. 2 the cross section  $\sigma(gg \rightarrow \phi \rightarrow \gamma\gamma)$  as a function of  $\xi$ . In the left plot we fix  $m_1^g = 3$  TeV and color-code according to the value of  $\Lambda_\phi$  while in the right plot we show the variation with  $m_1^g$  for each  $\Lambda_\phi$  curve. In both plots we also highlight the observed cross section bands from the ATLAS [1] and CMS [2] collaborations in the di-photon final state. These plots clearly show that the cross section  $\sigma(gg \rightarrow \phi \rightarrow \gamma\gamma)$  reaches a maximal value for conformal limit of  $\xi \sim 0.16$  and, more intriguingly, the region in the vicinity of this peak for  $\Lambda_\phi < 3$  TeV can, depending upon  $m_1^g$ , give the observed di-photon cross section of (5 – 15) fb. Note that the peak  $\gamma\gamma$  cross section occurs very close to the conformal point of  $\xi = 1/6$  for  $m_1^g \sim 5$  TeV and  $\Lambda_\phi \sim 2.5$  TeV. Further, this peak value roughly corresponds to the average of the ATLAS and CMS values. It is important to comment here that the  $\sigma(gg \rightarrow \phi \rightarrow \gamma\gamma)$  has a very small dependence the on

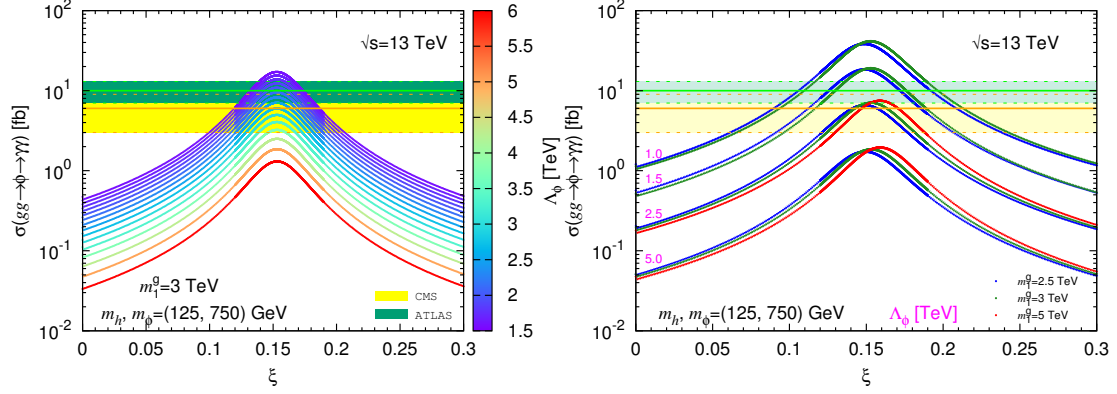


**Figure 2:** These graphs show the cross-section of the Higgs-radion  $\phi$  to  $\gamma\gamma$  through the gluon fusion,  $\sigma(gg \rightarrow \phi \rightarrow \gamma\gamma)$ , as a function of  $\xi$  for  $m_h = 125$  GeV,  $m_\phi = 750$  GeV and  $m_1^g = 3$  TeV with different choices of  $\Lambda_\phi$ . Whereas, the right plot shows the same as left but with different values of  $m_1^g$ . The observed cross section from the ATLAS [1] and CMS [2] Collaborations are displayed in light-green and yellow bands.

$m_1^g$  for a fixed value of  $\Lambda_\phi$ , see the right panel of Fig. 2. This implies that the maximal cross section will not significantly change when varying the  $m_1^g$  as long as the  $\Lambda_\phi$  is allowed by the EWPO, as illustrated in Fig. 1. In particular, even for a large  $m_1^g = 5$  TeV, this scenario can achieve the observed cross section with  $\Lambda_\phi = 2.5$  TeV.

Note that in the conformal limit  $\xi \simeq 1/6$  the Higgs-radion couplings to all the SM particles are suppressed, except to the massless gauge bosons  $\gamma\gamma$  and  $gg$ . One can easily see this behaviour from the couplings listed in Table 2. For instance, in the conformal limit  $\xi \simeq 1/6$ , the coupling parameters  $g_{h,\phi}$  and  $g_{h,\phi}^r$  defined in Table 2 take the following simple forms:

$$g_h \simeq \cos \theta, \quad g_\phi \simeq \sin \theta, \quad g_h^r \simeq \ell \sin \theta, \quad g_\phi^r \simeq -\ell \cos \theta. \quad (2.2)$$

Now for the case of  $m_h = 125$  GeV and  $m_\phi = 750$  GeV, in the conformal limit  $\xi \simeq 1/6$ , the mixing angle  $\theta$  is very small,  $\theta \approx \ell/36$ . Therefore, in the conformal limit the Higgs  $h$  couplings to the SM particles would be very much like the SM, while the Higgs-radion  $\phi$  couplings would be such that except  $\gamma\gamma$  and  $gg$ , all the other couplings become negligible  $\mathcal{O}(\ell^2/36)$ , see also Ref. [13]. This feature is manifestly reflected in the right panel of Fig. 3. There, we show the branching ratios of the Higgs-radion  $\phi$  decaying to  $XX = b\bar{b}, t\bar{t}, ZZ, hh, gg, \gamma\gamma, Z\gamma$ , as function of  $\xi$  for  $m_h = 125$  GeV,  $m_\phi = 750$  GeV and  $m_1^g = 3$  TeV. In the vicinity of  $\xi \approx 1/6$ , it is indeed reflected that  $gg$  and  $\gamma\gamma$  modes dominate the Higgs-radion decay. In the right panel of Fig. 3, we present the total width of the Higgs-radion  $\Gamma_\phi^{\text{tot}}$  at  $m_\phi = 750$  GeV. It shows that in the region of our interest  $\xi \approx 1/6$ , the total width is much smaller than the width observed by the ATLAS [1] and CMS [2] collaborations, which is around 45 GeV.

As pointed out in the Introduction due to a great enhancement in the  $gg$  decay compared to the  $\gamma\gamma$ , that has been observed in Fig. 3, one may be worried about a too large  $gg$  cross section, that might have been excluded by the di-jet search at the LHC. To address this concern, we present in Fig. 4 the cross-section of the Higgs-radion  $\phi$  to di-gluon  $gg$  through the gluon fusion (which is the dominant production channel),  $\sigma(gg \rightarrow \phi \rightarrow \gamma\gamma, gg)$ ,

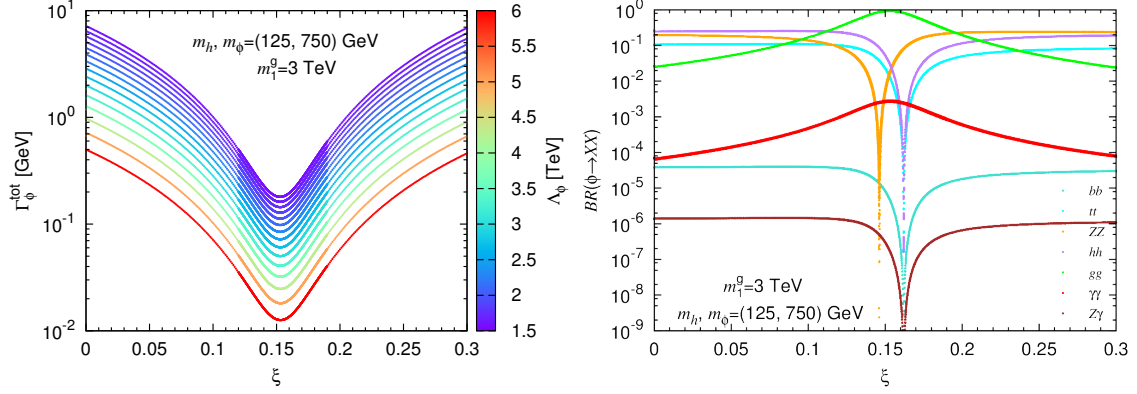


**Figure 3:** The left graph gives the total width of Higgs-radion  $\Gamma_\phi^{\text{tot}}$ , as function of  $\xi$  for  $m_h = 125$  GeV,  $m_\phi = 750$  GeV,  $m_1^g = 3$  TeV with different choices of  $\Lambda_\phi$ . Whereas the right graph shows the branching ratios of the Higgs-radion  $\phi$  going to  $XX = b\bar{b}, t\bar{t}, ZZ, hh, gg, \gamma\gamma, Z\gamma$ , as function of  $\xi$  for  $m_h = 125$  GeV,  $m_\phi = 750$  GeV and  $m_1^g = 3$  TeV.

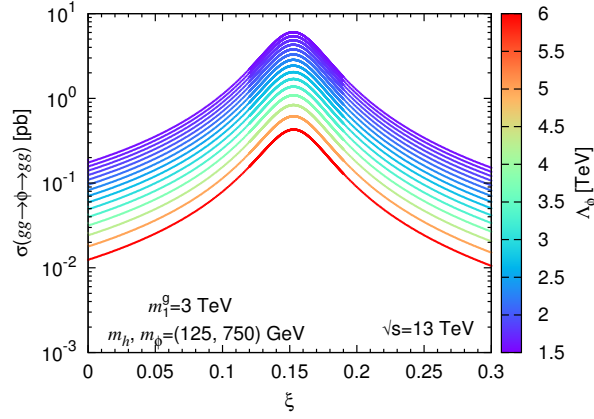


**Figure 4:** This graph shows the cross-section of the Higgs-radion  $\phi$  to  $gg$  through the gluon fusion,  $\sigma(gg \rightarrow \phi \rightarrow gg)$ , as function of  $\xi$  for  $m_h = 125$  GeV,  $m_\phi = 750$  GeV and  $m_1^g = 3$  TeV with color-coded by  $\Lambda_\phi$ .

analogous to Fig. 2. We focus on the region around the peak,  $\xi \approx 1/6$ , which predicts the  $\sigma(gg \rightarrow \phi \rightarrow gg) \leq 7$  pb. This is well below the experimental limits [17].<sup>1</sup> It is important to comment that in the near future with the increased sensitivity and more data accumulated the ATLAS and CMS collaborations will be able to observe the  $gg$  signals in this di-photon excess region if the Higgs-radion 750 GeV hypothesis we consider in this study is correct. Hence, the measurement of the cross section  $\sigma(gg \rightarrow \phi \rightarrow gg)$  is the prediction of the Higgs-radion 750 GeV scenario.

For the purpose of detecting this resonance in other channels, we also present in Fig. 5 the cross-section of the Higgs-radion  $\phi$  decaying to  $WW$ ,  $ZZ$  and  $Z\gamma$  final state, as function of  $\xi$ . As it can be seen from the graphs in Fig. 5 that near the conformal point all cross-sections of the Higgs-radion  $\phi$ , going to  $WW$ ,  $ZZ$  and  $Z\gamma$  final states, have suppression as noticed above.

<sup>1</sup>Here we rescaled the 8 TeV run-1 limit to the energy  $\sqrt{s} = 13$  TeV by a factor of  $\sim 5$ , leading to an upper bound around 10 pb.

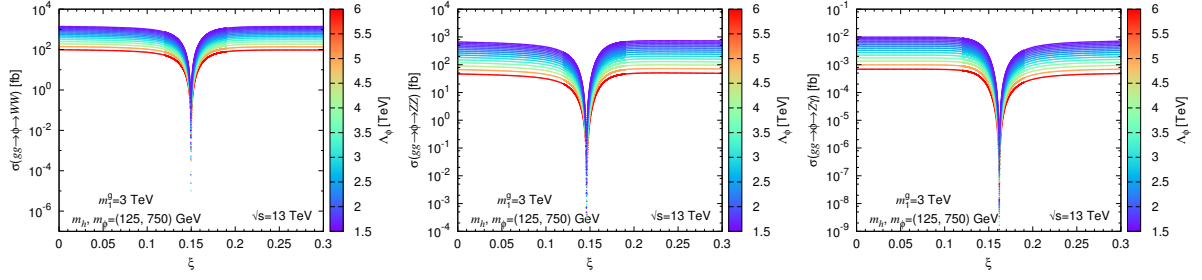


**Figure 5:** The above graphs show the cross-section of the Higgs-radion  $\phi$  decaying to  $WW$ ,  $ZZ$  and  $Z\gamma$ , as function of  $\xi$  for  $m_h = 125$  GeV,  $m_\phi = 750$  GeV,  $m_1^g = 3$  TeV with different choices of  $\Lambda_\phi$ .

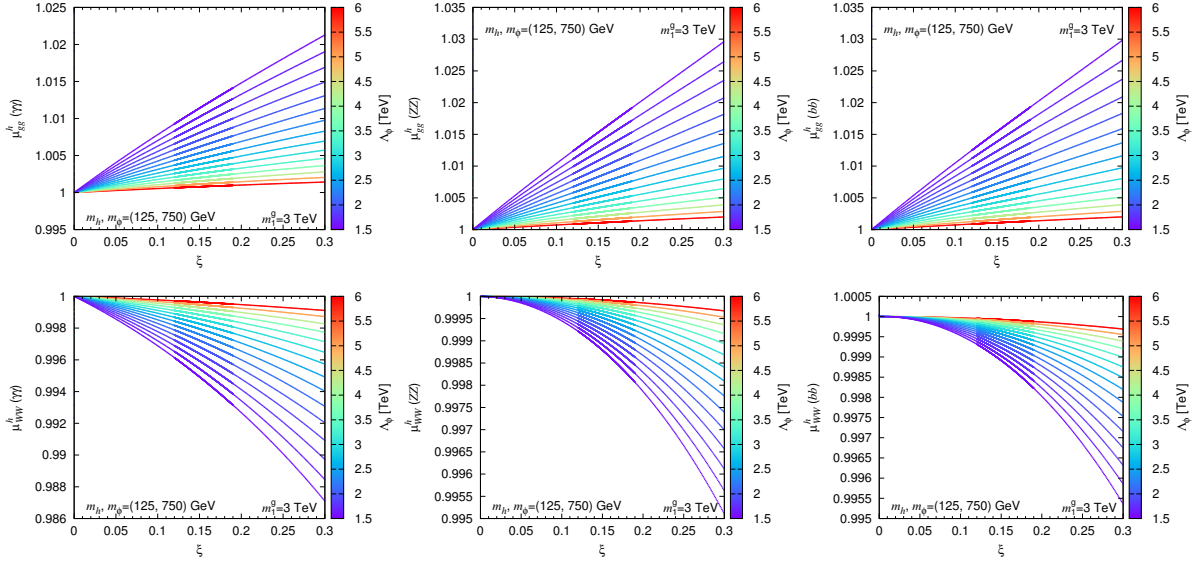


**Figure 6:** The above graphs show  $\mu_{gg}^h(XX) \equiv \sigma((gg, WW) \rightarrow h \rightarrow XX)/\sigma_{SM}((gg, WW) \rightarrow h \rightarrow XX)$ , where  $XX = \gamma\gamma, ZZ, b\bar{b}$  as function of  $\xi$  for  $m_h = 125$  GeV,  $m_\phi = 750$  GeV,  $m_1^g = 3$  TeV with different choices of  $\Lambda_\phi$ .  $\mu_{gg}^h(\gamma\gamma)$  and  $\mu_{gg}^h(ZZ)$  have a similar dependence on  $\Lambda_\phi$ .

It is needless to say that the Higgs-radion scenario must fit the Higgs data for 125 GeV state prior to the Higgs-radion interpretation of the newly observed state at 750 GeV. To this end, we examine the signal strength for all the measured channels. Figure 6 illustrates the  $\mu_{gg}^h(XX) \equiv \sigma(gg \rightarrow h \rightarrow XX)/\sigma_{SM}(gg \rightarrow h \rightarrow XX)$ , where  $XX = \gamma\gamma, ZZ, b\bar{b}$  as function of  $\xi$  for  $m_h = 125$  GeV,  $m_\phi = 750$  GeV,  $m_1^g = 3$  TeV with different choices of  $\Lambda_\phi$ . As expected the  $\mu_{gg}^h(XX) \equiv \sigma(gg \rightarrow h \rightarrow XX)/\sigma_{SM}(gg \rightarrow h \rightarrow XX)$  is very SM-like for  $\xi \approx 1/6$  and all the ratios we checked are consistent with the current Higgs data.

Finally, in Table 3 we collect five benchmark points (BMPs) for the Higgs-radion 750 GeV scenario for an interpretation of the recent di-photon excess at the LHC. Point-1 gives the maximal cross section in the  $\gamma\gamma$  (and simultaneously in the  $gg$ ) final state for  $m_1^g = 3$  TeV. For a larger  $m_1^g = 5$  TeV, points-2 and -3 show the maximal level at the different choices of  $k/M_{Pl}$ . It is obviously that all of these three points are positioned at the peak of each  $\Lambda_\phi$  curve. Next we examine how large the total width it could be when fitting the central values reported by ATLAS and CMS, which are given in Point 4 and 5,

respectively. Comparing points 1 and 3 we observe the effects of increasing  $m_1^g$  from 3 to 5 TeV, keeping  $k/M_{Pl}$  constant. As expected, we see a dramatic drop in the cross-sections to photons and gluons and in the total width. In point 2 we keep  $m_1^g$  at 5 TeV, but increase the  $k/M_{Pl}$  from 2 to 3. Due to a decrease in  $\Lambda_\phi$  we see that the total width and cross-sections are much larger than in the  $k/M_{Pl} = 2$  case, and are actually comparable to the case with  $m_1^g = 3$  TeV and  $k/M_{Pl} = 2$ . This is important, since if precision bounds or direct detection bounds push up the limits on  $m_1^g$ , this model can still reproduce the properties of the observed di-photon resonance at 750 GeV. In the last two points we demonstrate the effects of moving away from the conformal ( $\xi = 1/6$ ) limit. As expected, we see a decrease in the cross-sections to photons and gluons, however we see an increase in total width due to the increased branching ratios to  $W$  and  $Z$  bosons. This can be seen clearly from Fig. 2 and Fig. 3.

**Table 3:** Five benchmark points for the Higgs-radion 750 GeV scenario as an interpretation of the di-photon excess at the LHC. Below the dimensions for the dimensionful quantities are as:  $m_1^g$  [TeV],  $\Lambda_\phi$  [TeV],  $\Gamma_\phi^{\text{tot}}$  [GeV] and  $\sigma_{gg}^\phi(\gamma\gamma, gg)$  [fb].

BMP	$m_1^g$	$\xi$	$\Lambda_\phi$	$k/M_{Pl}$	$\Gamma_\phi^{\text{tot}}$	$\sigma_{gg}^\phi(\gamma\gamma)$	$\sigma_{gg}^\phi(gg)$	$\mu_{gg}^h(\gamma\gamma)$	$\mu_{gg}^h(ZZ)$	$\mu_{WW}^h(ZZ)$
1	3	0.153	1.5	2	0.2	18.92	6.68	1.013	1.017	0.999
2	5	0.159	1.67	3	0.15	16.39	5.77	1.01	1.015	0.999
3	5	0.159	2.5	2	0.068	7.49	2.58	1.005	1.006	1.000
4	3	0.13	1.5	2	0.375	9.99	3.6	1.011	1.015	0.999
5	3	0.117	1.5	2	0.622	6.02	2.19	1.01	1.013	0.999

### 3 Conclusions

In this work we have studied the phenomenology of a heavy radion from the RS model, and argued that this state could be responsible for the recent excess in the di-photon channel observed at ATLAS and CMS. A crucial feature in this model is the mixing between the radion field and the Higgs field, introduced via a coupling of the Higgs field to gravity parameterized by the mixing parameter  $\xi$ . For values of  $\xi$  close to the conformal limit,  $\xi = 1/6$ , one finds that the Higgs-like mass eigenstate  $h$  (with  $m_h = 125$  GeV imposed) has very SM-like couplings, while couplings of the radion-like mass eigenstate  $\phi$ , with  $m_\phi = 750$  GeV, to gluons and photons are enhanced and its couplings to other fields are very small. The model can easily accommodate the observed cross-section in the di-photon channel while remaining within run 1 constraints and satisfying all other constraints such as those from electroweak precision measurements, bounds on the lightest KK excitation, and so forth. The main problem for this scenario is that the total width of the  $\phi$  can only be as large as  $\sim 0.1$  GeV if we are to avoid too much suppression of the di-photon branching ratio, whereas the estimated width from ATLAS and CMS is  $\sim 45$  GeV. This model also predicts a large cross-section for  $gg \rightarrow \phi \rightarrow gg$  that is only just below current limits. Thus, once further data is taken, an absence of a signal in this channel would rule out this model.

## Acknowledgements

The work of AA and BG has been supported in part by the National Science Centre (Poland) as research project no DEC-2014/13/B/ST2/03969. B.M.D. was supported by the Science and Technology Facilities Council (UK). J.F.G. is supported in part by the US DOE grant DE-SC-000999 and he also acknowledges the University of Warsaw for hospitality. Y.J. acknowledges generous support by the Villum Foundation.

## A Holographic interpretation: a 750 GeV dilaton

The simple RS model has a natural interpretation in terms of a strongly coupled CFT in 4D, where the conformal symmetry is spontaneously broken by the formation of bound states at some IR scale. In the 5D model this IR scale is indicated by the position of the IR brane, and the KK modes from the 5D model are to be interpreted as the bound states breaking the CFT in the 4D model.

The radion, associated with the fluctuation in the inter-brane distance, has a natural interpretation in 4D as the dilaton, the goldstone mode of the spontaneously broken conformal symmetry. Whereas the fluctuations in the 4D metric components of Eq. (1.1), usually thought of in terms of KK gravitons, can be thought of as spin-2 glueballs of the 4D CFT. The most general effective Lagrangian one can write down for a dilaton in 4D is of the form,

$$\begin{aligned} \mathcal{L}_{eff} = & \frac{1}{2} \partial_\mu h_0 \partial^\mu h_0 + \frac{1}{2} (1 + a_1 \ell^2) \partial_\mu \phi_0 \partial^\mu \phi_0 \\ & - \frac{1}{2} m_h^2 h_0^2 - \frac{1}{2} m_\phi^2 \phi_0^2 - a_2 \ell \partial_\mu \phi_0 \partial^\mu h_0 - a_3 \ell m_\phi^2 \psi_0 h_0. \end{aligned} \quad (\text{A.1})$$

The  $a$  parameters are related to certain features of the 5D model. The parameters  $a_3$  and  $m_\phi^2$  parameterise the explicit conformal symmetry breaking in the 4D model, without which the dilaton is massless. In 5D this is directly related to the back-reaction on the metric which perturbs the AdS curvature, and when there is no back-reaction the radion is massless. In 5D models the  $a_1$  parameter is also related to the back-reaction on the metric, however its presence does not break the conformal symmetry. In any generic model one would expect  $a_{1,2,3}$  to be non-zero. However in composite Higgs models this argument is complicated slightly by the fact that  $a_2$  and  $a_3$  explicitly break the shift symmetry of the goldstone Higgs, see also Ref. [18] in the light of recent di-photon excess at the LHC. So in these cases it is sometimes assumed that these effects only arise at loop level.

Lastly, the parameters in the effective Lagrangian in Eq. A.1 can be related to our parameters via,

$$a_1 = a_2 = 6\xi, \quad a_3 = 0. \quad (\text{A.2})$$

The reason  $a_3 = 0$  is that we have a brane Higgs, thus a mass mixing does not arise through the Higgs-gravity coupling  $\xi \mathcal{R} H^\dagger H$  on the IR brane. If we wanted to include this effect it would have to be put in by hand. With a bulk Higgs however  $a_3 \neq 0$  would arise naturally from the Higgs-gravity coupling.



## B Electroweak precision constraints on $m_1^g$

In this work we assume a custodial symmetry ( $SU(2)_L \times SU(2)_R$ ) in the bulk, broken to the SM subgroup on the UV brane. This helps to suppress large corrections to the  $T$  parameter. In these models the largest constraint arises from the  $S$  parameter, given by,

$$\delta S \simeq 2\pi \frac{v^2}{m_{KK}^2} \simeq 12\pi \frac{v^2}{(m_1^g)^2}, \quad (\text{B.1})$$

where we define  $m_{KK} = ke^{-\frac{1}{2}kb_0}$  and we use the relation  $m_1^g \simeq \sqrt{6}m_{KK}$ . This model is attractive due to the fact that  $\delta T \simeq 0$ , however  $T$ -parameter corrections can arise from several sources; loops of KK tops, a small bulk breaking of  $SU(2)_R$ , radion loops, or corrections to the SM Higgs contribution. Assuming a maximal value for the  $T$  parameter the bound from electroweak precision observables is  $S \lesssim 0.3$ . This implies a lower bound on the mass of the lightest spin-1 resonance,  $m_1^g \sim 2.8$  TeV.

Because we have an enlarged global symmetry, we must introduce new fields to embed the SM quarks in full representations. These additional fields will naturally be heavy since  $SU(2)_R$  is broken on the UV brane, giving these fields Dirichlet boundary conditions and thus no zero mode. Following [12], the contribution from KK tops to  $T$  can be written as,

$$\begin{aligned} \delta T_{KK\text{tops}} &\simeq 0.7 \delta T_{SM\text{top}} \left( \frac{4}{(1-2c_L)^2} \frac{1}{(j_{-c_L+0.5})^2} \right) \frac{m_t^2}{m_{KK}^2} \\ &\simeq 5 \left( \frac{4}{(1-2c_L)^2} \frac{1}{(j_{-c_L+0.5})^2} \right) \frac{m_t^2}{(m_1^g)^2} \end{aligned} \quad (\text{B.2})$$

where  $\delta T_{SM\text{top}} \simeq 1.2$  is the SM contribution, the 0.7 factor comes from the KK sum and a numerical integration,  $0.1 \lesssim c_L \lesssim 0.4$  is the 5D mass of the left handed doublet, and  $j_x$  is the first zero of the Bessel function  $J_x$ . If we have a bulk breaking of the  $SU(2)_R$  symmetry, the contribution to the  $T$  parameter is,

$$\delta T_b \simeq \frac{3\pi kb_0}{2s_w^2} \left( \frac{\tilde{M}}{2k} \right)^2 \frac{v^2}{(m_1^g)^2}, \quad (\text{B.3})$$

where the free parameter  $\tilde{M}$  is a bulk mass parameter that controls the size of the  $SU(2)_R$  breaking in the bulk. Between this contribution and the contribution from the KK tops, a sizeable correction to the  $T$  parameter can be generated in order to give the bound  $S \lesssim 0.3$ .

The contribution from the modified Higgs couplings and from the radion field are more involved, and the calculation has only yet been done in the scenario with all SM fields on the IR brane [9, 19]. In these works it is shown that for a small mixing parameter  $\xi$ , the effects on the EWPOs are under control. However an in depth study with bulk gauge and fermion fields is required. One major difference between having bulk gauge fields rather than brane localised gauge fields, is that there is an additional suppression in the coupling of the radion to massive gauge fields,

$$\left( 1 - 3kb_0 \frac{M_V^2}{\Lambda_\phi^2} \right) \frac{\phi_0}{\Lambda_\phi} V^\mu V_\mu, \quad (\text{B.4})$$

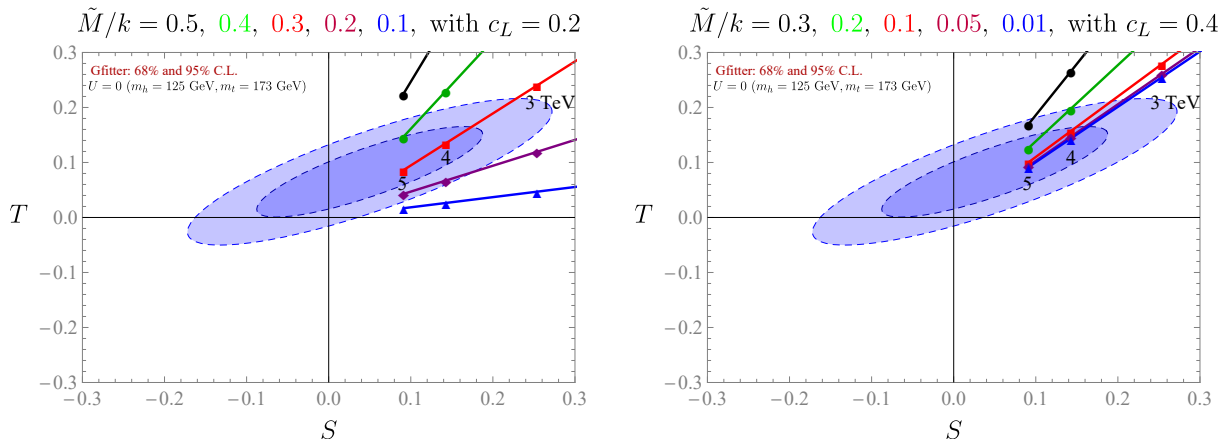


**Figure 7:** These plots show the EWP constraints on  $m_1^g$  for different choices of bulk top-quark mass parameter  $c_L$ , see Appendix B. Above different curves are chosen for different values of the bulk gauge boson mass parameter  $\tilde{M}$ , which breaks the bulk custodial symmetry.

note that here we have taken  $\xi = 0$ . This could have a non-negligible effect on the precision analysis.

Since the custodial symmetry gives us some control over the contribution to the  $T$  parameter, the most important corrections from the Higgs-radion sector will be to the  $S$ -parameter. Even a contribution of  $+0.1$  pushes the lower bound on the lightest spin-1 resonance from  $\sim 2.8$  TeV to  $\sim 4.8$  TeV. Small negative contributions, such that  $S$  is still positive, will result in the dominant bounds being from direct detection ( $\sim 2.5$  TeV). Whereas large negative corrections, such that  $S$  becomes negative, would be the most constrained case, see Fig. 7.

## References

- [1] **ATLAS** Collaboration, G. Aad et al., *Search for high-mass diphoton resonances in  $pp$  collisions at  $\sqrt{s} = 13$  TeV with the ATLAS detector*, ATLAS-CONF-2015-081.
- [2] **CMS** Collaboration, S. Chatrchyan et al., *Search for High-Mass Diphoton Resonances in  $pp$  Collisions at  $\sqrt{s} = 13$  TeV with the CMS Detector*, CMS PAS EXO-15-004.
- [3] L. Randall and R. Sundrum, *A Large mass hierarchy from a small extra dimension*, *Phys.Rev.Lett.* **83** (1999) 3370–3373, [[hep-ph/9905221](#)].
- [4] W. D. Goldberger and M. B. Wise, *Modulus stabilization with bulk fields*, *Phys.Rev.Lett.* **83** (1999) 4922–4925, [[hep-ph/9907447](#)].
- [5] O. DeWolfe, D. Freedman, S. Gubser, and A. Karch, *Modeling the fifth-dimension with scalars and gravity*, *Phys.Rev.* **D62** (2000) 046008, [[hep-th/9909134](#)].
- [6] D. Dominici, B. Grzadkowski, J. F. Gunion, and M. Toharia, *The Scalar sector of the Randall-Sundrum model*, *Nucl. Phys.* **B671** (2003) 243–292, [[hep-ph/0206192](#)].
- [7] D. Dominici, B. Grzadkowski, J. F. Gunion, and M. Toharia, *Higgs Boson interactions within the Randall-Sundrum model*, *Acta Phys. Polon.* **B33** (2002) 2507–2522, [[hep-ph/0206197](#)].



- [8] B. Grzadkowski, J. F. Gunion, and M. Toharia, *Higgs-Radion interpretation of the LHC data?*, *Phys. Lett.* **B712** (2012) 70–80, [[arXiv:1202.5017](#)].
- [9] C. Csaki, M. L. Graesser, and G. D. Kribs, *Radion dynamics and electroweak physics*, *Phys. Rev.* **D63** (2001) 065002, [[hep-th/0008151](#)].
- [10] M. Toharia, *Higgs-Radion Mixing with Enhanced Di-Photon Signal*, *Phys. Rev.* **D79** (2009) 015009, [[arXiv:0809.5245](#)].
- [11] P. Cox, A. D. Medina, T. S. Ray, and A. Spray, *Radion/Dilaton-Higgs Mixing Phenomenology in Light of the LHC*, *JHEP* **02** (2014) 032, [[arXiv:1311.3663](#)].
- [12] K. Agashe, A. Delgado, M. J. May, and R. Sundrum, *RS1, custodial isospin and precision tests*, *JHEP* **08** (2003) 050, [[hep-ph/0308036](#)].
- [13] G. F. Giudice, R. Rattazzi, and J. D. Wells, *Graviscalars from higher dimensional metrics and curvature Higgs mixing*, *Nucl. Phys.* **B595** (2001) 250–276, [[hep-ph/0002178](#)].
- [14] K. Agashe, H. Davoudiasl, G. Perez, and A. Soni, *Warped Gravitons at the LHC and Beyond*, *Phys. Rev.* **D76** (2007) 036006, [[hep-ph/0701186](#)].
- [15] CMS Collaboration, *Search for  $t\bar{t}$  resonances in semileptonic final state*, *CMS-PAS-B2G-12-006* (2012).
- [16] ATLAS Collaboration, *A search for  $t\bar{t}$  resonances in the lepton plus jets final state with ATLAS using  $14\text{ fb}^{-1}$  of  $pp$  collisions at  $\sqrt{s} = 8\text{ TeV}$* , *ATLAS-CONF-2013-052* (2013).
- [17] ATLAS Collaboration, G. Aad et al., *Search for new phenomena in the dijet mass distribution using  $p - p$  collision data at  $\sqrt{s} = 8\text{ TeV}$  with the ATLAS detector*, *Phys. Rev.* **D91** (2015), no. 5 052007, [[arXiv:1407.1376](#)].
- [18] R. Franceschini, G. F. Giudice, J. F. Kamenik, M. McCullough, A. Pomarol, R. Rattazzi, M. Redi, F. Riva, A. Strumia, and R. Torre, *What is the  $\gamma\gamma$  resonance at  $750\text{ GeV}$ ?*, [arXiv:1512.04933](#).
- [19] J. F. Gunion, M. Toharia, and J. D. Wells, *Precision electroweak data and the mixed Radion-Higgs sector of warped extra dimensions*, *Phys. Lett.* **B585** (2004) 295–306, [[hep-ph/0311219](#)].